International Journal of Biological Macromolecules 164 (2020) 3474–3484

Contents lists available at ScienceDirect

International Journal of Biological Macromolecules

journal homepage: http://www.elsevier.com/locate/ijbiomac

Reversible and irreversible fluorescence activity of the Enhanced Green Fluorescent Protein in pH: Insights for the development of pH-biosensors

Nathalia Vieira dos Santos [a,b], Carolina Falaschi Saponi [a,b], Timothy M. Ryan [c], Fernando L. Primo [a], Tamar L. Greaves [b], Jorge F.B. Pereira [a,d,*]

[a] Department of Engineering of Bioprocesses and Biotechnology, School of Pharmaceutical Sciences, São Paulo State University (UNESP), Rodovia Araraquara-Jaú/Km 01, 14800-903 Araraquara, SP, Brazil
[b] School of Science, College of Science, Engineering and Health, RMIT University, 124 La Trobe Street, Melbourne, VIC 3000, Australia
[c] Australian Synchrotron, 800 Blackburn Road, Clayton, VIC 3168, Australia
[d] Univ Coimbra, CIEPQPF, Department of Chemical Engineering, Rua Sílvio Lima, Pólo II – Pinhal de Marrocos, 3030-790 Coimbra, Portugal

ARTICLE INFO

Article history:
Received 18 May 2020
Received in revised form 9 July 2020
Accepted 28 August 2020
Available online 31 August 2020

Keywords:
Green Fluorescent Protein
Protein stability
Fluorescence
Small-angle X-ray scattering (SAXS)
Circular dichroism (CD)
Intrinsic fluorescence of proteins
Biosensor

ABSTRACT

Enhanced Green Fluorescent Protein (EGFP) is a biomolecule with intense and natural fluorescence, with biological and medical applications. Although widely used as a biomarker in research, its application as a biosensor is limited by the lack of in-depth knowledge regarding its structure and behavior in adverse conditions. This study is focused on addressing this need by evaluating EGFP activity and structure at different pH using three-dimensional fluorescence, circular dichroism and small-angle X-ray scattering. The focus was on the reversibility of the process to gain insights for the development of biocompatible pH-biosensors. EGFP was highly stable at alkaline pH and quenched from neutral-to-acidic pH. Above pH 6.0, the fluorescence loss was almost completely reversible on return to neutral pH, but only partially reversible from pH 5.0 to 2.0. This work updates the knowledge regarding EGFP behavior in pH by accounting for the recent data on its structure. Hence, it is evident that EGFP presents the required properties for use as natural, biocompatible and environmentally friendly neutral to acidic pH-biosensors.

1. Introduction

Green Fluorescent Protein (GFP) is a biomolecule with intense and natural fluorescence, which can be easily quantified and evaluated, allowing its application as a biomarker and biosensor [1,2]. However, although GFP and other fluorescent proteins are widely used in research as biomarkers [3], there is a lack of in-depth knowledge regarding the structure and behavior in different environments of many of its variants, such as temperature and pH, which is the basis for a wider development of biosensors [4,5]. For example, only recently the crystalline structure of the most popular recombinant GFP (variant Enhanced GFP, EGFP) was elucidated [6,7], and none of the previous pH studies with EGFP accounted this data for the variant [8–10]. Therefore, crucial information for understanding and predicting EGFP behavior at different pH is still missing, and studies of reversible modifications of this protein are essential to improve its current use as a biosensor and for the development of novel applications for EGFP.

The first fluorescent protein, known as wild-type GFP (wtGFP), was originally isolated from the jellyfish *Aequorea victoria* [2]. Today, wtGFP can be expressed by a series of organisms, like *Escherichia coli* (*E. coli*) and *Caenorhabditis elegans* [1], and is extensively used as a biomarker [11]. In its native form, the fluorophore of wtGFP is located inside a β-barrel scaffold, formed by 11 β-strands and one central α-helix [12], as can be seen in Fig. 1A. The fluorophore of wtGFP is formed by the autocatalytic cyclization of the tripeptide –Ser65-Tyr66-Gly67, which confers two peaks of fluorescence with maximum intensity at the excitation wavelengths of 395 nm for the protonated states of the protein (higher intensity peak) and 475 nm for its deprotonated state (lower intensity peak) [11,13]. Despite its intense and natural fluorescence, wtGFP presents two main disadvantages for biological applications, of 1) its inefficient folding above 20 °C [14] (below the optimal temperature for most microorganisms and cells used in research, like *E. coli*, yeast and mammalian cell cultures [15,16]), and 2) its low intensity of fluorescence when excited at higher wavelengths (which are preferred over lower wavelengths that can damage biological samples) [11,14]. To overcome these limitations, recombinant variants of wtGFP were developed, including EGFP (mutations F64L and S65T) [17], which presented improved folding above 20 °C and high fluorescence intensity when excited at higher wavelengths [2,11].

* Corresponding author at: Univ Coimbra, CIEPQPF, Department of Chemical Engineering, Rua Sílvio Lima, Pólo II – Pinhal de Marrocos, 3030-790 Coimbra, Portugal.
E-mail address: jfbpereira@eq.uc.pt (J.F.B. Pereira).

https://doi.org/10.1016/j.ijbiomac.2020.08.224
0141-8130/

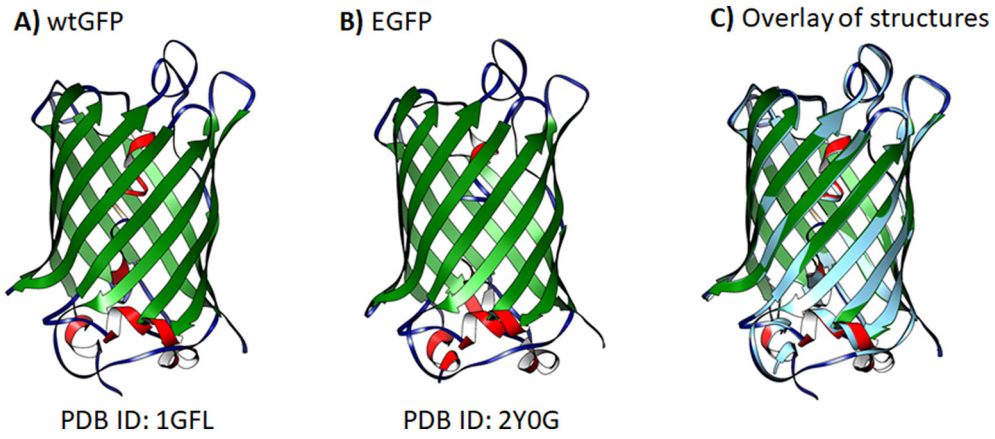

Fig. 1. A) Representation of the crystalline structure of the *Aequorea victoria* wtGFP expressed by *E. coli*, PDB ID: 1GFL. B) Representations of the crystalline structure of EGFP expressed by *E. coli*, PDB ID: 2Y0G. Helix are presented in red, strands in green and coils in blue. C) Overlay of wtGFP structure (in colour) and EGFP (in gray). Images were produced with the PDB structures [18] using UCSF Chimera 1.14. [19].

Nowadays, EGFP variant is one of the most used fluorescent proteins [20], but much about its behavior is still under investigation. For example, it was originally stated that EGFP presented only the deprotonated state as a result of favored S65T mutation [6,21]. However, after the elucidation of its crystalline structure (PDB ID: 2Y0G [7] and 4EUL [6], as shown in Fig. 1B), it was noted that, similar to wtGFP, the variant EGFP also present both protonated and deprotonated states. The minor differences between the structures of EGFP and wtGFP can be seen in Fig. 1C, mostly small alterations in the position of coils and helix in the extremities of the protein. Hence, although there is literature on the stability of EGFP at different pH [8–10], the previous studies were not aware of the presence of these two states for this protein, or did not address the structural effects of pH on the protein. Therefore, there is a need to reexamine the effect of pH on the structure and behavior of EGFP, with a focus on how, and especially if, EGFP could be used for the development of pH-biosensors.

Each GFP variant is stable over a different pH range. For example, wtGFP is stable between pH 5.5 and 12.0 [14], with a pKa of 4.5 [2]. Whereas EGFP has a pKa of 6.0 [17], is less stable at acidic pH, and more resistant to alkaline pH. The wtGFP has a low sensitivity to acidic pH (*viz.* higher resistance to pH-induced fluorescence quenching), while EGFP and GFP-S65T have a moderate sensitivity [10], and other GFP variants such as pHluorin and pHluorin2 a high sensitivity [22]. The loss of fluorescence due to pH is not always undesirable for fluorescent proteins, and in the case of pHluorin and pHluorin2 [22], their low resistance to acidic pH allows their application in the monitoring of intracellular pH [8,22]. Additionally, changes to the environment of the fluorescent proteins can lead to reversible and irreversible changes to their fluorescence activity [11] – a crucial phenomenon for the development of pH-biosensors [23,24].

Biosensors for medical applications are essential tools to detect and monitor a series of diseases, and there is a great demand for them with the increased focus on prevention over remediation of health issues [25]. Because of their high sensitivity, fluorescent compounds are particularly useful in the development of sensors [26–28]; however, there are concerns that need to be addressed for the selection of fluorophores for pharmaceutical formulations [25]. Although inorganic fluorophores are easier to work with than fluorescent proteins, their toxicity is a barrier for medical use. The toxicity of fluorescence dyes have been reported decades ago [29], and more recently, cytotoxicity at low concentrations was also reported on novel fluorophores like quantum dots [30,31]. Fluorescent proteins have been extensively applied for biological studies, including *in vivo* assays, being biocompatible with cells and animals, and presenting very low toxicities [11,32,33], making them well suited for use in pharmaceutical formulations. Additionally, fluorescent proteins are also biodegradable and environmentally friendly, not presenting the same risks and difficulties in disposal as some other organic and heavy metals-based fluorophores [34].

Biocompatible pH-biosensors are particularly interesting for the medical field, because some diseases are known to alter the pH around the afflicted areas. For example, the region around tumors usually presents a more acidic pH than healthy tissues (with the average pH for tumors around 7.0, and for healthy tissues around 7.4) [35,36]. Similarly, there is a relationship between the acidic pH of synovial fluids and a variety of joint diseases [37]. However, it should also be noted that these applications are also dependent on the development of novel technologies, as for example, devices capable of subtracting the background autofluorescence of tissues and biological materials which could interfere with GFP fluorescence on *in vivo* experiments. A successful example is the technology developed by Wack et al. to monitor pancreatic tumors in mice, using GFP in a whole-body imaging system [38]. Hence, there is great potential for pH-biosensors to diagnose and monitor different diseases, and low toxicity is an essential requirement for their medical applications and commercial use.

Additionally, we believe that there are other unexplored fields for fluorescent protein application, which could benefit from more fundamental studies about their structure and behavior in aqueous solutions. Particularly for EGFP, a recent work demonstrated the potential of this GFP variant for developing novel environmentally friendly luminescent solar concentrators, yielding power conversion efficiencies up to 30% higher than the traditional systems commercially available [39].

Considering this information, the present work evaluated the fluorescence and structure of EGFP at different pH, using three-dimensional fluorescence spectroscopy (3D fluorescence), circular dichroism (CD), spectroscopy of the intrinsic fluorescence of proteins (IFP) and small angle X-ray scattering (SAXS) in well-plates or with size-exclusion chromatography (SEC-SAXS). All techniques were applied to elucidate the effects and processes associated with protein unfolding and refolding at different pH. This in-depth study of EGFP stability in varying pH, and the evaluation of the relationship between EGFP fluorescence and pH, provides important information for the development of biomarker and biosensor applications of this low-toxic, and natural alternative, to other fluorophores, such as dyes and quantum dots.

2. Methods

2.1. Materials

Potassium Phosphate Buffer (PB) 10.0 mM pH 7.4 and Phosphate-Saline Buffer (PBS) pH 7.4 (137.0 mM NaCl, 2.7 mM KCl, 8.0 mM

Na_2HPO_4 and 2.0 mM KH_2PO_4) were selected to simulate physiological conditions, considering that the main use of EGFP is in the medical and biological fields. The PB 10.0 mM pH 7.4 was prepared with MilliQ water, anhydrous dipotassium hydrogen phosphate (K_2HPO_4, 98–100.5%) from QHEMIS and anhydrous monopotassium hydrogen phosphate (KH_2PO_4, 99%) from Synth (Brazil). PBS was prepared with tablets from Sigma-Aldrich® and MilliQ water. The pH of the buffer was corrected using 3 M solutions of phosphoric acid (H_3PO_4, 85 wt% in H_2O) and potassium hydroxide (KOH, 45 wt% in H_2O), both from Sigma-Aldrich®. Other reactants used in this study were acquired from Sigma-Aldrich® and used as received. EGFP with >97.5% purity was produced and purified using the method previously developed by the group and published by dos Santos et al. [40].

2.2. pH stability of EGFP

The first set of experiments evaluated the fluorescence intensity of EGFP in PBS at different pH (2.0, 3.0, 4.0, 5.0, 6.0, 7.0, 7.4, 8.0, 9.0, 10.0, 11.0, 12.0 and 13.0) over time (0, 0.5, 1, 2, 3, 4, 5, 6, 24 and 48 h). Then, EGFP in PB solution was exposed to different pH (from 2.0 to 9.0) for 30 min (time required for fluorescence stabilization at the new pH conditions) and evaluated by CD and fluorescence spectroscopy (3D and single point for GFP fluorophore and 2D for intrinsic fluorescence of proteins). Then, the pH of each sample was adjusted until the solution reached neutrality (pH 7.4), and after 60 min, EGFP was again assessed by CD and fluorescence analysis.

The relationship between fluorescence intensity of EGFP and pH was also evaluated. Fluorescence intensity (in units of fluorescence, UF) single points were obtained for twelve different pH from 5.0 to 8.0 at F1 (λ_{ex} 488 nm, λ_{em} 510 nm), in triplicate with a blank using an EnSpire® Multimode Plate Reader, from PerkinElmer®.

2.3. Fluorescence analysis

The 3D fluorescence emission spectra and fluorescence intensity single points were acquired at 25 °C with a concentration of 5.4 $\mu g \cdot mL^{-1}$ ([5.4 $\mu g \cdot mL^{-1}$ (200 pM)]) of EGFP, using a spectrofluorophotometer RF-6000 SHIMADZU® for 3D spectra and a multimode plate reader (EnSpire® Multimode Plate Reader, PerkinElmer®) for the single points. The 3D fluorescence spectra of the fluorophore were acquired with a variable wavelength range of excitation (λ_{ex}) from 240 to 550 nm and emission (λ_{em}) from 470 to 570 nm (interval of 2.0 nm for λ_{ex} and 1.0 nm for λ_{em}, scan speed 6000 $nm \cdot min^{-1}$, λ_{ex} bandwidth 10.0 nm and λ_{em} bandwidth 1.0 nm). From the 3D spectra, it was possible to extract emission and excitation curves for EGFP. The fluorescence intensity points were obtained in triplicate with a blank with 10 ms accumulation time at F1 λ_{ex} 488, λ_{em} 510 nm, the wavelength of highest fluorescence intensity of EGFP in PB pH 7.4, as can be seen in Fig. S1 in the SI. Considering EGFP bleaching half-life of 174 s [41] and the low accumulation time (10 ms), the experiment was designed to prevent photobleaching in the single point analysis. EGFP in PBS pH 7.4 0 h was the reference for 100% for the calculation of Relative FI (%). Results were evaluated in triplicate with a blank and presented as mean ± standard deviation.

The intrinsic fluorescence of proteins (IFP, given by the presence of the amino acids Tyr, Trp, and phenylaniline, Phe) [42] can also indicate variations in protein conformation and structure. Their contribution was evaluated by emission spectra in the λ_{ex} 280 nm and λ_{em} range from 290 to 410 nm (Tyr and Trp residues), with a scan speed of 200 $nm \cdot min^{-1}$, λ_{ex} bandwidth of 3.0 nm and λ_{em} bandwidth of 5.0 nm. For the emission spectra of the intrinsic fluorescence of proteins, the data was adjusted so that the FI of the last emission point (at λ_{em} 410 nm) of each sample was 0 UF after subtraction of the blank (spectra of PB). Experiments were performed in triplicate with a blank.

2.4. pH and conductivity calibration and determination

The pH (±0.003) and conductivity (±1.0% $mS \cdot cm^{-1}$) at 25 (±1) °C of the samples were measured using a portable pH meter and conductometer Metrohm®/Model 914, calibrated with standard buffers for pH (values of 7.00 and 4.01) and standard solution of KCl (0.1 $mol \cdot dm^{-3}$) for conductivity. The pH of each sample was adjusted with 3 M solutions of KOH and H_3PO_4 (±0.1).

2.5. Circular dichroism (CD) analysis

The secondary structure of EGFP was obtained using CD with a J-1500 spectrometer from Jasco®. The spectra were acquired at 25 °C in triplicate with a blank, using a cell of 1 mm, scan speed 100 $nm \cdot min^{-1}$, wavelength from 300 to 190 nm, interval of 1.0 nm, 6 accumulations, Digital Integration Time (D.I.T.) of 4 s, bandwidth of 1.00 nm and concentration of 0.3 $mg \cdot mL^{-1}$ (11 μM) of EGFP. The High Tension (HT) was maintained below 700 to obtain a reliable CD signal. Experiments were performed in triplicate with a blank. CD analysis was only conducted using the PB buffer since the chlorine ions present in PBS solution are incompatible with CD.

CD results are presented as mean residue ellipticity ([θ]). The [θ] was calculated using the following Eq. (1): [43].

$$[\theta] = \frac{(\theta * MRW)}{(P * C)} \quad (1)$$

where θ is the CD value (mdeg), MRW is the Mean Residue Weight of the protein, P is the path length of the CD cell in mm and C is the concentration of the protein in $mg \cdot mL^{-1}$.

MRW was calculated for EGFP following the Eq. (2): [43].

$$MRW = \frac{MW\ protein\ (Da)}{(n\ of\ amino\ acid\ residues - 1)} \quad (2)$$

EGFP has a MW of 26.9 kDa and 239 amino acid residues, with an MRW of 113.025 ($Da \cdot res^{-1}$). P was 1 mm and C was 0.3 $mg \cdot mL^{-1}$.

For the data processing, according to the critical review on CD from Greenfield 2009 [43], most CD analysis software have difficulties in predicting the secondary structure of proteins which are majorly formed by β-strands, like EGFP. The most accurate results were obtained with K2D and CONTIN programs. Considering K2D only predicts the percentage of β-strands and α-helix, while CONTIN can also calculate turns and make distinctions between regular and distorted β-strands and α-helix, Dichroweb with CONTIN [44,45] set SP175 (optimized for the range of 190–240 nm) [46] was used for the CD data analysis.

2.6. Small-angle X-ray scattering (SAXS)

The SAXS experiments were performed at the SAXS/WAXS beamline of the Australian Synchrotron (ANSTO), Melbourne, Australia, using two techniques which provided distinct information regarding EGFP behavior at different pH: well-plate SAXS and Size Exclusion Chromatography SAXS (SEC-SAXS). The SEC-SAXS is a newly developed SAXS technique for the analysis of biomolecules (BIOSAXS), which combines SAXS with size-exclusion chromatography (SEC) and a co-flow system, allowing scattering patterns to be acquired continuously on the different fractions of the protein sample [47]. Considering that EGFP is a weak dimer [2], the protein can be found as a monomer, dimer or even as aggregates, hence, the SEC-SAXS can provide information regarding the structure of the protein and the aggregates at different speciation. The well-plate SAXS was also evaluated because, although it is from scattering from all the EGFP monomers and aggregates, and hence lower quality data than SEC-SAXS, it can give information about samples that are not suitable for SEC-SAXS, including samples with

precipitates (for example, denatured proteins or protein solutions with pH close to its pI). For SEC-SAXS, patterns were acquired while the sample was flowed through a capillary, to minimize protein degradation. The protein solution was under constant flow surrounded by a sheath of the corresponding solvent, and is a technique suitable for weakly-scattering protein samples, minimizing protein denaturation from prolonged X-ray radiation. It has been designed to enable high quality data with excellent background subtraction, which is suitable to comparison with protein models to obtain information about the tertiary structure of the protein [47,48]. The capillary was washed between samples, and the same location on the capillary was used for all measurements to maximize accuracy in subtracting the solvent. The q range selected for SAXS was 0.006 to 0.53 $Å^{-1}$. Details regarding sample preparation, data collection parameters, use of software and structural parameters can be found in Table S3 from the SI. Advanced technical specifications for the equipment can be found in ANSTO website [49]. SAXS software scatterbrain 2.82 from ANSTO [50], ATSAS [51] and SREFELX [52] were used for SAXS data analysis. The EGFP PDB ID 2Y0G [7,53] structure (Fig. 1B) was used as a model for the SAXS fittings.

2.6.1. Well-plate SAXS

An initial test for concentrations 0.5, 1.0, 2.0, 2.5, 3.0, 4.0 and 5.0 $mg \cdot mL^{-1}$ (respectively 18.6, 37.2, 74.3, 92.9, 111.5, 148.7, 185.9 μM) of EGFP were evaluated to find the lowest concentration which provided a strong and clear scattering signal. The concentration of 2.5 $mg \cdot mL^{-1}$ (92.9 μM) of EGFP was selected. Samples were prepared in buffer PB with pH adjusted to pH 4.0, 5.0, 6.0 and 7.4 and after 30 min, scattering in SAXS was measured. Then, pH of the samples was adjusted to 7.4 and after 60 min, were evaluated by SAXS again. Experiments were performed with a blank and 15 measurements were recorded for each sample. The q range was 0.006 to 0.53 $Å^{-1}$. Results are presented as the average of measurements after blank subtraction of the corresponding solvent.

2.6.2. Sec-SAXS

The SEC-SAXS associates the SAXS technique with a High-performance liquid chromatography (HPLC), using a size-exclusion column GE Healthcare® Superdex s200. Equipment and procedures followed Ryan et al. specifications [47]. PB of pH 7.4, 6.5 and 5.5 were used as eluent for the HPLC column, and filtered with an 0.5 μm membrane. This pH range was selected because below pH 5.5 (due to loss of structure) and around pH 6 (due to it being close to the pI of the protein) there is precipitation, making the sample not suitable for SEC-SAXS. 50 μL of sample was injected per run, with a flow rate of 0.4 $mL \cdot min^{-1}$. The HPLC column was equilibrated for 15 min for each eluent and the run was recorded for UV (wavelengths 214 nm, 260 nm, 280 nm and 450 nm) and SAXS for 15 min per sample. A concentration test with samples with 2.0, 2.5, 3.0, 5.0 and 10 $mg \cdot mL^{-1}$ (respectively 74.3, 92.9, 111.5, 185.9 and 371.7 μM) of EGFP were performed to find the lowest concentration which provided a strong and clear scattering signal. The concentration of 5.0 $mg \cdot mL^{-1}$ (185.9 μM) of EGFP was selected. The samples were prepared with PB with the same pH as the eluents and injected in SEC-SAXS after 30 min. For the presentation of the results, time was manually adjusted so the SEC-SAXS peaks from the samples at different pH matched, considering the time of injection varied for each condition. The offset used for the SEC-SAXS results was then applied for the time adjustment for the Rg, MW, and UV results.

3. Results and discussion

3.1. Fluorescence activity of EGFP in function of pH and time

The first set of assays evaluated the fluorescence activity from pH 2.0 to 13.0 over 48 h for the highest intensity peak of EGFP (F1, wavelength of excitation (λ_{ex}) 488 nm wavelength of emission (λ_{em}) 510 nm). Table S1 from the SI presents the real pH and conductivity measurements of the samples from Fig. 2. As shown in Fig. 2, the fluorescence of EGFP was maintained in aqueous solutions with pH between 7.0 and 13.0. When the pH was 6.0 and below, the fluorescence was significantly reduced. At pH 6.0, EGFP lost around half of its relative Fluorescence Intensity (FI) (%) when compared to EGFP at pH 7.4. At pH 5.0, there was a decrease of more than 80% of EGFP fluorescence, and at pH 4.0 and below, fluorescence was fully suppressed.

3.2. Study of the reversibility of fluorescence activity of EGFP in pH

The second set of experiments aimed to infer if the fluorescence quenching of EGFP in neutral to acidic pH was reversible. For that purpose, the EGFP was exposed to different pH for 30 min, followed by 60 min at pH 7.4. The exposure time of 30 min to the different pH was selected since the fluorescence of EGFP was mainly stabilized after this period (as can be seen in Fig. 2). In addition, the goal was to evaluate properties for the development of biosensors with quick responses. The pH 7.4 was selected as the control (reference for neutral pH), pH 8.0 and 9.0 were chosen to evaluate the effect of alkalinity (considering there was almost no difference in fluorescence from pH 8.0 to 13.0). Furthermore, pH of 2.0, 3.0, 4.0, 5.0 and 6.0 were selected to assess the impact of acidity on EGFP structure, given the greater sensitivity of the protein to lower pH values. Firstly, EGFP in potassium phosphate

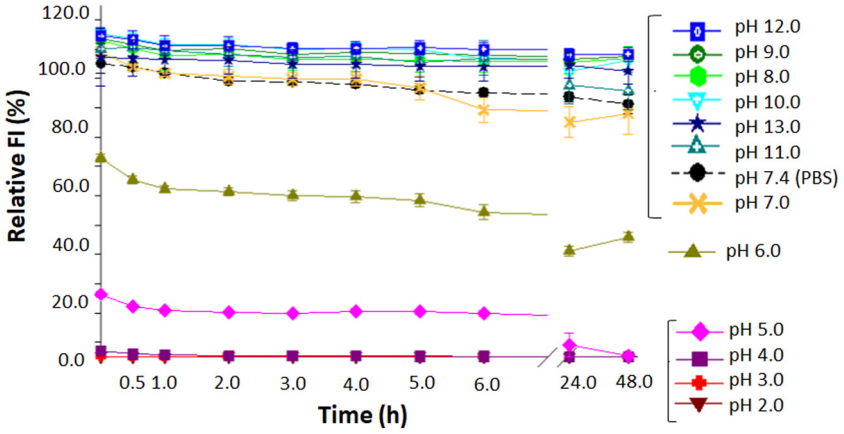

Fig. 2. Effect of pH in EGFP relative fluorescence intensity (FI) (%) over time (48 h). EGFP [5.4 $\mu g \cdot mL^{-1}$ (200 pM)] in PBS 0 h is the reference for 100%. Results were evaluated in triplicate with a blank and presented as mean ± standard deviation.

buffer (PB) solutions were exposed to the different pH for 30 min and the point fluorescence and 3D fluorescence spectra were acquired. Secondly, the pH of each EGFP solution was adjusted to reach neutrality (pH 7.4), and after 60 min of stabilization, the EGFP fluorescence activity was assessed again.

The reversibility of the pH-induced fluorescence loss for the highest FI point of EGFP (F1) is shown in Fig. 3, where the black bars represent the relative FI (%) after 30 min at the different pH, and the red bars indicate the intensity after returning to pH 7.4. The relative FI (%) of EGFP decreased around 30% after 30 min at pH 6.0 (reaching 67.2 ± 0.9%); however, 60 min after returning to pH 7.4 the relative FI returned to 80.3 ± 0.5%. In contrast, the fluorescence of EGFP after 30 min at pH 5.0 decreased to 28.8 ± 0.1%, and only 55.3 ± 0.5% of relative FI was regained after 60 min at pH 7.4. The fluorescence of EGFP was effectively quenched after 30 min exposure to pH 4.0, 3.0 or 2.0, and the fluorescence was restored up to 42.8% after 60 min returning to pH 7.4 (42.8 ± 0.4%, 38.8 ± 0.4% and 25.2 ± 0.3% of relative FI for pH 4.0, 3.0 and 2.0, respectively).

Considering wtGFP presents a pH-dependent fluorescence for its protonated and deprotonated states [2], the 3D spectra of EGFP was also evaluated to verify if this phenomenon was also present for the enhanced variant. The 3D spectra can simultaneously assess excitation and emission curves for the protein, and can indicate if blue or red shifts are occurring. The 2D spectra (emission and excitation) are shown in Fig. S4, and the complete 3D spectra in Figs. S2 and S3 of the SI, which overall provide a more complete representation of the effects of pH on EGFP fluorescence. The results presented in Figs. S4, S2 and S3 are consistent with those shown in Fig. 3, with fluorescence quenching after 30 min of exposure to pH below 7.4. This again was followed by a small return of fluorescence for pH 2.0 to 5.0, and an almost complete return of fluorescence for pH 6.0 after the pH was adjusted to neutrality for 60 min. The maximum FI of EGFP was achieved at pH 8.0 for F1, as shown in Figs. S4.A, S4·C and S2. No changes or shifts in the shape of the spectra, or the maximum excitation and emission wavelengths, were observed at the different pH, though the FI varied as previously shown in Figs. 2 and 3. Relatively to EGFP at pH 7.4, Figs. S4.A and S4·C show there was a slight increase of fluorescence at pH 8.0 and 9.0, while a fluorescence quenching was observed at pH 6.0 and below (with greater fluorescence decrease for lower pH values). After the return to pH 7.4, as shown in Figs. S4·B and S4.D, the samples previously kept at pH 6.0 had their fluorescence restored, while the ones at pH 5.0 presented only a partial recovering of fluorescence. On the other hand, the samples kept at pH ≤4.0 had a very low return of FI, as proven by both the EGFP emission and excitation spectra.

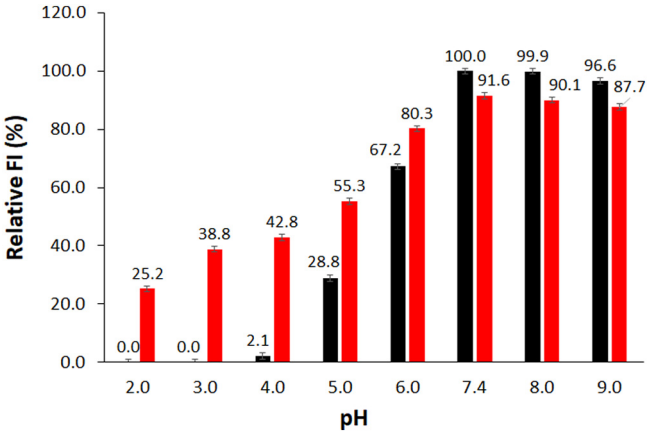

Fig. 3. Effect of pH in EGFP relative fluorescence intensity (FI) (%) after 30 min exposure to different pH (black bars ■), followed by return to pH 7.4 for 60 min (red bars ■). EGFP [5.4 μg·mL^{-1} (200 pM)] in PBS 0 h is the reference for 100%. Results were evaluated in triplicate with a blank and presented as mean ± standard deviation.

3.3. Structural alterations of EGFP in function of pH

To obtain further insights behind the EGFP fluorescence reversibility with pH, the effect of pH on the secondary and tertiary structure of EGFP was analyzed using CD, IFP, well-plate SAXS and SEC-SAXS. As in the previous experiments, EGFP in PB solutions were exposed to the different pH for 30 min and CD, IFP, well-plate SAXS and SEC-SAXS were evaluated. Then, the pH of each EGFP solution was adjusted to reach neutrality (pH 7.4), and after 60 min, EGFP was again assessed with the aforementioned techniques.

The effects of pH on EGFP secondary structure were evaluated using CD spectroscopy, and the results are presented in Fig. 4. In CD spectroscopy, α-helix presents negative bands at 222 nm and 208 nm, and a positive band at 193 nm, while β-helices have a negative band at 218 nm and a positive band at 195 nm [43]. EGFP secondary structure at neutral pH is already reported in literature, [6] being comprised of 47% of β-strands (11 strands forming a β-barrel core, with the chromophore located in its center), 13% of helical forms (3_{10} and α conformations, with the core helix containing the chromophore) and 40% of coils (mostly from loops located at the two ends of the β-barrel structure). As can be seen in Fig. 4A, from pH 5.0 to 9.0, there is a negative ellipticity observed from around wavelength 205 to 240 nm (negative band for α-helix at 222 nm and 208 nm, negative band for β-strands at 218 nm) and positive ellipticity from 190 to 205 nm (positive band for α-helix at 193 nm and positive band for β-strands at 195 nm). The CD spectra at Fig. 4A for pH 5.0 to 9.0 matches other CD studies for EGFP [54,55]. However, at pH 5.0, there was a decrease in both positive and negative ellipticities, suggesting that the protein suffered secondary structural changes at this condition. From pH 2.0 to 4.0, there are clearly further alterations, not only in the intensity, but in the shape of the spectra, consistent with modifications to the secondary structure of EGFP. The CD spectra of the samples after returning to the neutral pH of 7.4 for 60 min are shown in Fig. 4B. The EGFP which was exposed to pH 5.0 partially recovered its ellipticities, and similarly, EGFP exposed to pH 2.0, 3.0 or 4.0 had their positive and negative ellipticities and intensities partially restored. However, the samples exposed to these lower pH values had lower intensities relative to the EGFP maintained at pH 7.4, with EGFP exposed to pH 5.0 being closest in intensity and shape to EGFP in pH 7.4.

In Fig. 4C and D, and Table S1 from the SI, the results for the CD analysis with Dichroweb CONTIN-LL (set SP175) are presented. As can be seen in Fig. 4C and Table S1, the results for EGFP at pH 7.4 match very closely with the previous reports for the crystalline structure of EGFP at neutral environments [6], as confirmed by the 1% variation for the calculated β-strands and helical forms, respectively 48% and 12% for this study, *versus* 47% and 13% for EGFP crystalline structure described in literature [6], confirming the accuracy of our CD data analysis. This set was then selected for subsequent studies of the effect of pH on EGFP secondary structure and recovery after pH neutralization. In Fig. 4C, it is possible to see there are no modifications on the secondary structure of EGFP from pH 6.0 to 9.0. On the other hand, from pH 5.0 to 2.0, there is an incremental decrease on β-strands and an increase on unordered structures of EGFP. Although the modifications on overall helical forms are small (Fig. 4C), Table S2 shows that with the decrease of pH, the percentage of distorted α-helix is higher than at neutral and alkaline pH. From Fig. 4D, with the return of pH to neutrality, it is possible to observe that EGFP almost, but not completely, recovers its secondary forms after being exposed to pH 5.0, while only a partial recovery occurs for pH values ≤4.0. At acidic pH values (≤4.0), EGFP still has a higher proportion of unordered forms and distorted α-helix, with only a partial recovery of β-strands. The CD data is helpful for understanding why less than 50% of EGFP FI returns after the pH adjustment to neutrality.

The IFP was also evaluated for information on the effect of pH on EGFP, as presented in Fig. 5. The IFP provides information about the conformation and stability of proteins, because the fluorescence of certain amino acids [namely, tryptophan (Trp), tyrosine (Tyr) and

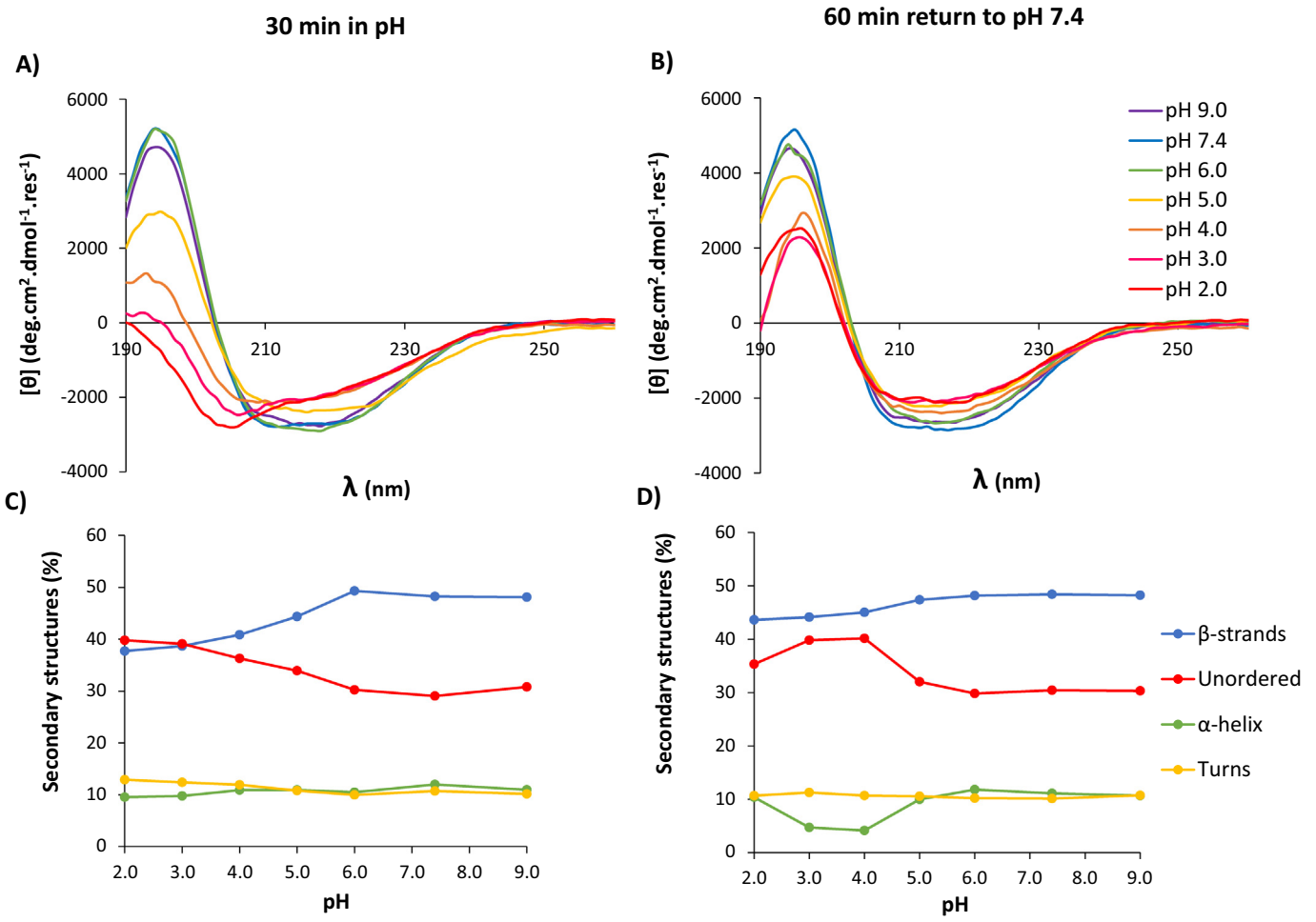

Fig. 4. Mean residue ellipticity ([θ]) from the CD analysis of EGFP (0.3 mg·mL^{-1} (11 μM), 1 mm cell) in PB of different pH after A) 30 min exposure to different pH and B) 30 min exposure to different pH + 60 min return to pH 7.4. Percentage (%) of secondary structures of EGFP (CD analysis in Dichroweb CONTIN-LL, set SP175) after C) 30 min exposure to different pH and D) 30 min exposure to different pH + 60 min return to pH 7.4. Samples were prepared in triplicate with a blank and presented as the average of the results.

phenylalanine (Phe)] are strongly influenced by their surrounding environment and position in the protein structure [56]. The emission of the Tyr residues can be affected by proton loss, rotational motions in the protein and the presence of quenching groups close to the protein. Hence, these alterations in fluorescence can provide information about structural changes in the protein surface [56]. As can be seen in Fig. 5A, in general, the shape of the spectra and the maximum peaks for the IFP of EGFP after 30 min at different pH was not changed. The exception was the EGFP exposed to a pH of 2.0, where the shape of the emission spectra was altered. The FI of the IFP changed according to the pH, following the trend previously observed in the fluorescence and CD studies, with a decrease of intensity with decreasing pH. This effect was expected considering a change in the surround environment can alter the IFP because it modifies the exposure of the fluorescent

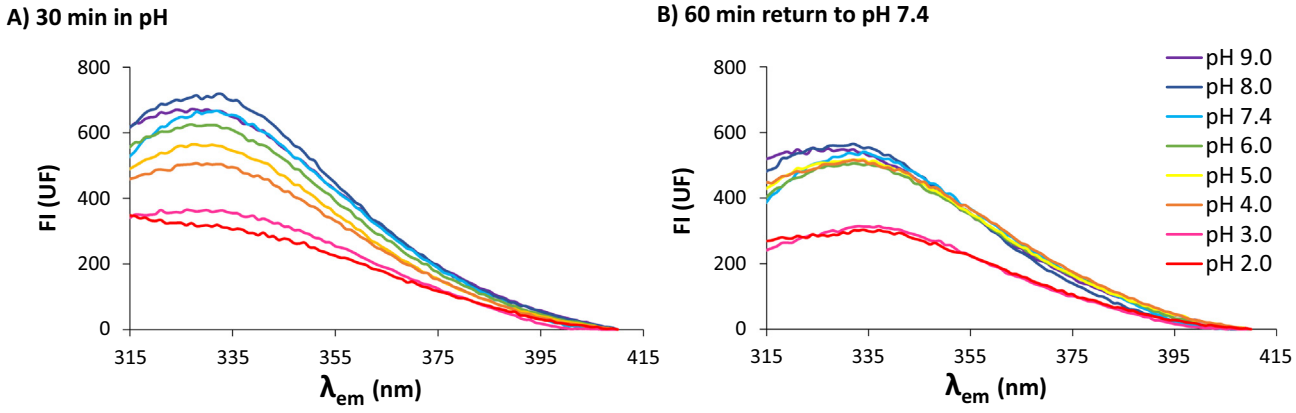

Fig. 5. Emission spectra of fluorescence of tyrosine and tryptophan of EGFP [5.4 μg·mL^{-1} (200 pM)] at excitation wavelength of 280 nm after A) 30 min exposure to different pH and B) 30 min exposure to different pH + 60 min return to pH 7.4. Data presented as fluorescence intensity (FI) in unities of fluorescence (UF).

amino acids. However, on returning all samples to pH 7.4 in Fig. 5B, the intensity of the IFP should return if the structure of the protein goes back to its usual form. This return was observed for pH 4.0 to 9.0, but not for pH 2.0 and 3.0. This suggests the alterations for pH 2.0 and 3.0 were too severe, and even with the neutralization of pH, the arrangement of the protein and the fluorescent amino acid residues did not return to the same position as in the properly folded EGFP. The results suggest there is a partial maintenance of the secondary structure of EGFP, which allows an incomplete recovery of some amino acid positioning, even after exposure to very acidic pH (pH 3.0 and 2.0). Additionally, although there is only a partial return of activity for EGFP after exposure to pH 4.0, there is enough structural restoration to recover amino acid positioning. However, as observed in CD, there are permanent alterations in secondary structure elements, which in turn, reduce the chromophores capacity to emit fluorescence.

To evaluate the effect of pH on EGFP tertiary structure, two SAXS techniques were applied: well-plate SAXS and SEC-SAXS. SAXS can provide data regarding the structure and structural transition of biomolecules in solution, but for accurate determination, monodisperse and dilute samples are required [47]. In the SEC-SAXS technique, the use of chromatography to separate different species from polydisperse solutions allows the evaluation of complex biological samples, as for example, proteins in different solvents or in solutions with distinct pH [47]. However, although SEC-SAXS can provide better resolution and more accurate information on EGFP as a monomer, this method is not appropriate for samples with large aggregates, as for example those with pH close to the pI, or denatured proteins. Hence, to obtain broader information on the behavior of EGFP after 30 min at different pH, both methods were used. Additionally, EGFP after 60 min return to pH 7.4 was evaluated on the well-plate SAXS.

The results for the well-plate SAXS are shown in Fig. 6. Since q is inversely proportional to real space, scattering at lower q are associated with larger specimens in the samples, while higher q is related to scattering of smaller species. The inclination at low q (below log q 0.06 $Å^{-1}$) in Fig. 6 for all conditions indicates the presence of aggregates for all the samples in the well-plate SAXS. Considering EGFP is a weak dimer prone to aggregation [2,9] and the concentration is high [2.5 mg·mL^{-1} (92.9 μM)], the presence of species with different sizes was expected, and was the reason why SEC-SAXS was also evaluated for clearer data on the structure and distribution of the different formations where possible. Because of the heterogeneity of the species in Fig. 6, it was not possible to fit the scattering to models, but the behavior of EGFP at different pH could still be assessed.

In Fig. 6A, it can be seen that the EGFP at pH 5.0, 6.0 and 7.4 had effectively identical scattering, except for variation in the larger aggregates at low q, where it appears that the proportion of aggregates present increased with decreasing pH. This indicates that, at pH 5.0 and 6.0, the overall structure of EGFP is maintained, but the formation of associations and aggregates is favored. For EGFP at pH 6.0, the aggregation could be due the proximity to the pI of the protein (6.2) [57], and not necessarily because of structural alterations. For EGFP at pH 4.0, there is not only the formation of aggregates at lower q, but the shape of the scattering at higher q was also altered, confirming structural changes of EGFP. After the return to pH 7.4 (Fig. 6B), there was a decrease in larger formations for both pH 5.0 and 6.0, with the latter presenting a scattering almost identical to EGFP at pH 7.4. However, for EGFP at pH 4.0, the return to pH 7.4 led to greater differences between this sample and the EGFP maintained at pH 7.4. This suggests that, at pH 5.0 and 6.0, EGFP mostly retains its tertiary structure with aggregation more favorable than at pH 7.4, while at pH 4.0 there was extensive structural modifications in the EGFP structure. This is in accordance to the previous fluorescence and CD studies, and can explain why EGFP can fully recover its fluorescence activity after exposure to pH 6.0, while there is only a partial recovery for pH 5.0 and even lower for pH 4.0.

The SEC-SAXS were acquired continuously on all fractions through the HPLC as a function of time. The average intensity of each SAXS pattern over time is provided in Fig. S5 of the SI. The EGFP at pH 7.4 was chosen as the neutral control, and pH 6.5 was selected instead of pH 6.0 to avoid the pI of EGFP (pH 6.2) [57], because proteins precipitate at the pI and could clog the HPLC column. The pH 5.5 was selected instead of 5.0 and 4.0 because EGFP starts precipitating at these lower pH values.

As was previously stated, EGFP is a weak dimer [2], and in addition to its monomeric form, it can appear as dimers or other associations at higher concentrations. The highest average intensity of the SAXS patterns around frame 250 in Fig. S5A, represents the monomeric EGFP, the peak between frames 200 and 250 is from the EGFP dimer, and the plateau between frames 150 and 200 is attributed to larger associations or aggregates. The scattering in Fig. S5A for pH 7.4 and 6.5 is very similar, with a slight decrease in dimers for pH 6.5. However, there is a large decrease in the proportion of dimers and aggregates for pH 5.5, and there is also alteration to the shape of the monomeric EGFP. Although usually higher concentrations of aggregates are associated with lower protein stability [58], considering the alterations to EGFP monomer, this could represent an intense stress at pH 5.5, which dissociated aggregates and also altered the structure of the protein.

The radius of gyration (Rg) and molecular weight (MW) were obtained for each SAXS pattern and are provided in Fig. S5B and C, respectively, for the EGFP sample after going through the HPLC column. The x-axis is the same for Fig. S5A, B and C, to allow comparison. The broad range of Rg and MW values for EGFP at pH 7.4 indicates a heterogeneity in species sizes in the sample, with the larger species eluting first. Although the EGFP at pH 6.5 generally matches EGFP at pH 7.4

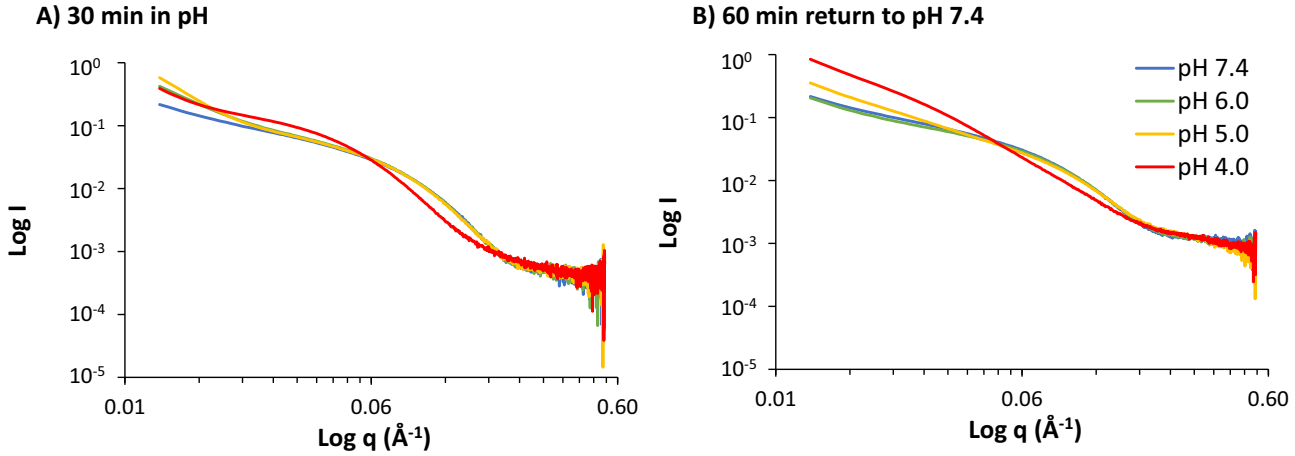

Fig. 6. Well-plate SAXS of EGFP [2.5 mg·mL^{-1} (92.9 μM)] after A) 30 min exposure to different pH and B) 30 min exposure to different pH + 60 min return to pH 7.4. Results are presented in log of intensity (Log I) and log of q ($Å^{-1}$).

for frames between 250 and 300, there are sections missing for this pH. The pH of 6.5 was chosen in an attempt to minimize precipitation near the pI of EGFP of 6.2 [57]. However, this data suggests the difference of 0.3 in pH was not enough to avoid the precipitation. Therefore, the missing sections for Rg and MW for EGFP at pH 6.5 are attributed to aggregation due to pI proximity. For EGFP at pH 5.5, the Rg and MW do not match those seen for EGFP at pH 7.5. There is a narrower dispersion of Rg values than at 6.5, indicating less aggregates are present. The MW of EGFP is 26.9 kDa [6], which is consistent with the plateau around frames 250 and 200 for EGFP monomer at pH 7.4 and 6.5, but there is no clear plateau in MW for EGFP at pH 5.5.

The HPLC allows the monitoring of the UV absorbance (A) of the samples simultaneously to the SEC-SAXS acquisition. Similar to the IFP, amino acids also have absorbance spectra and these can provide insight about alterations to the protein structure or its environment [59,60]. The absorbances at λ 214 nm, 260 nm, 280 nm and 450 nm are shown in Fig. S5D. The λ of 214 nm is associated with Phe absorbance, while 260 nm and 280 nm are related to Tyr and Trp absorbances. The λ of 450 nm was chosen to detect EGFP absorbance. As can be seen in Fig. S5D.1, D.2 and D.3, pH 7.4 and pH 6.5 exhibited similar absorbance as a function of time, with some reduction in intensity of pH 6.5 for the 450 nm absorbances (as shown in Fig. S5D.4). In contrast, EGFP at pH 5.5 had an absence of the first two peaks at 214 nm, and the absence of the first peak for 260 nm, 280 nm and 450 nm (Fig. S5D). These alterations indicate changes to the chromophore (due to the 450 nm spectra) and for amino acid environment/positioning (due to changes of lower wavelengths spectra) at pH 5.5, in accordance with the previous results observed in this study.

The SAXS scattering, structure of EGFP, p(r) and Rg for the monomeric fraction of EGFP at different pH after SEC-SAXS are presented in Fig. 7. The SAXS scattering for the monomeric EGFP fraction of samples exposed for 30 min to pH 7.4, 6.5 and 5.5 are shown in Fig. 7A. The corresponding p(r) are shown in Fig. 7B, which presents similar size distributions for EGFP at pH 7.4 and 6.5. However, on reducing the pH to 5.5, the distribution is skewed to larger sizes. The SAXS patterns were fitted to EGFP using PDB ID 2Y0G [7], and refined using SREFLEX [52]. Snapshots of these structures are provided in Fig. 7C, comparing the refined structures (cyan) to the 2Y0g PDB structure (green). The EGFP structure at pH 7.4 overall matched well to the PDB file, and was similar to the PDB file at pH 6.5. However, at pH 5.5, strands around the β-barrel are loosened and the barrel appears to be slightly "squashed". Additionally, the Rg for the EGFP at pH 7.4 (20.37 Å) [61] is very similar to reports for the monomeric variation of EGFP (m-EGFP, Rg of 20.29 ± 1.00 Å), but there is an increase on the Rg at pH 6.5 (21.46 Å) and pH 5.5 (23.32 Å). This suggests there were modifications on EGFP tertiary structure after 30 min at pH 5.5, which can be responsible for the fluorescence activity decrease (in comparison with pH 7.4.

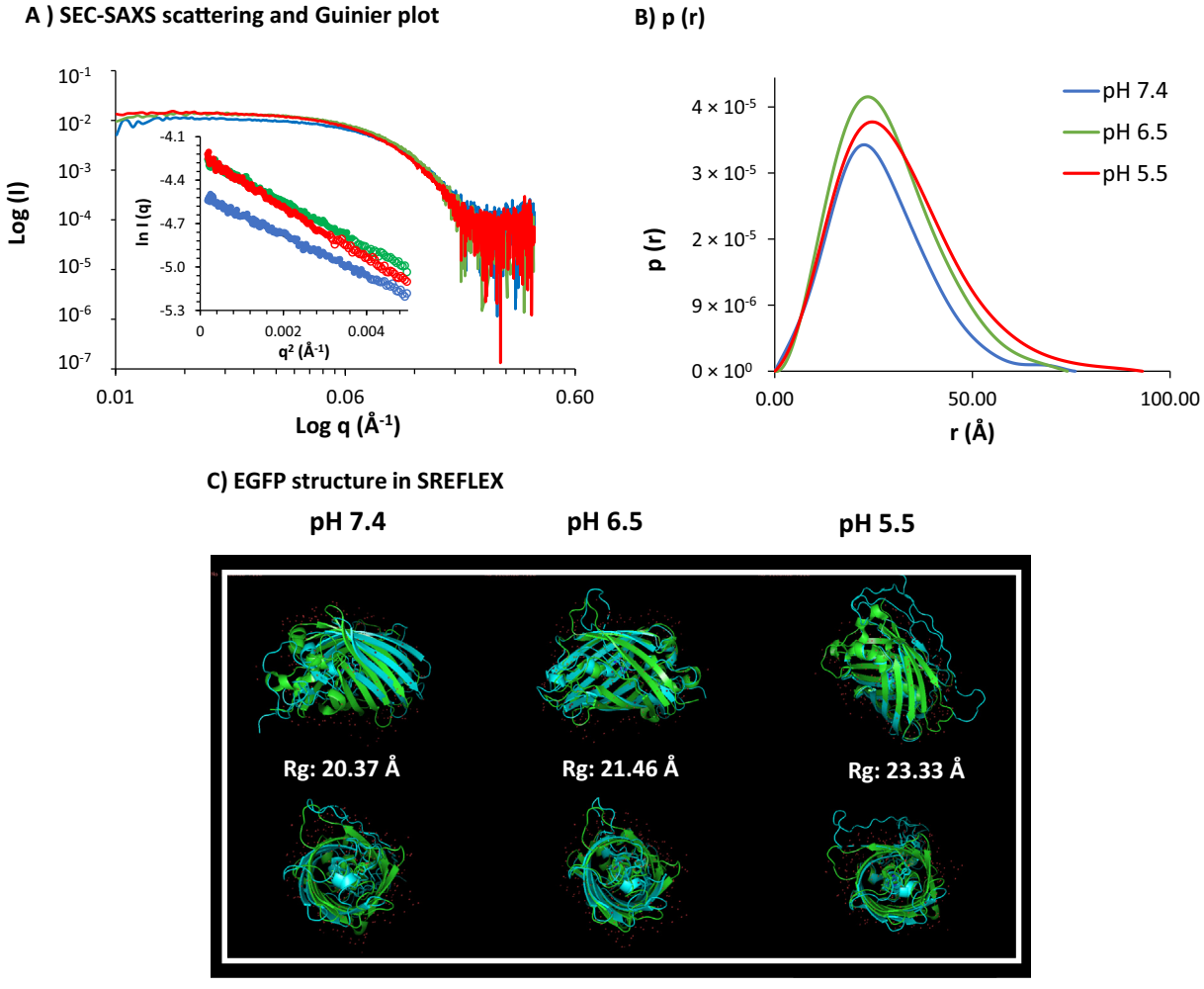

Fig. 7. Analysis of the monomeric fraction of EGFP [5 mg·mL^{-1} (185.9 μM)] from SEC-SAXS. A) SEC-SAXS and Guinier plot of EGFP after 30 min exposure to different pH. Results are presented in log of intensity (Log I) and log of q (Å^{-1}) for SAXS and natural log of intensity of q [ln I (q)] and q^2 (Å^{-1}) for the Guinier plot. B) p(r) of EGFP after 30 min at different pH. C) Radius of gyration (Rg) and images of monomeric EGFP structure after 30 min at different pH. Structures generated in SREFLEX using SEC-SAXS scattering and fittings to EGFP PDB ID 2Y0G file [7]. The top images are the lateral view of EGFP structure and the bottom images are the overview. EGFP PDB ID 2y0G shown in Green and refined fit to data shown in Cyan.

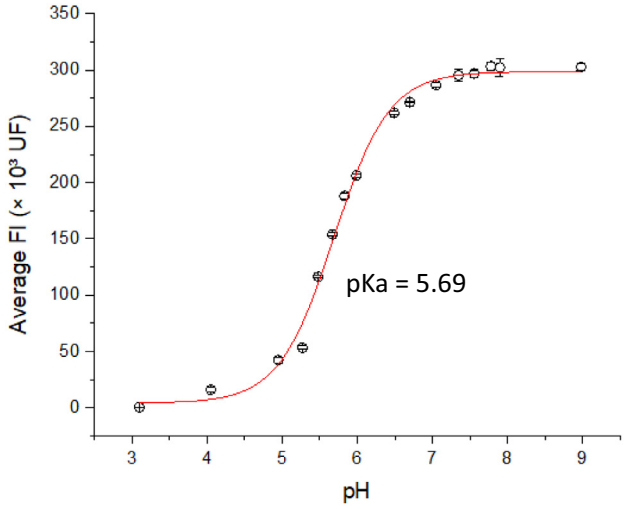

Fig. 8. Average Fluorescence Intensity [FI, $\times 10^3$ unities of fluorescence (UF)] of EGFP (5.4 μg·mL^{-1}) over pH. FI was acquired at EGFP peak (F1, λ_{ex} 488 nm, λ_{em} 510 nm) in triplicate with a blank. Results were fitted to a growth/sigmoidal dose response model to calculate pKa.

3.4. Impacts of pH on the activity and structure of EGFP

Allying the results from the fluorescence activity with the structural studies, it is possible to infer that EGFP is highly stable towards alkaline pH (7.4 to 13.0), lightly quenched from neutral to weakly acidic pH (8.0 to 5.0, with pKa 5.69) and heavily quenched below pH 5.0 (5.0 to 2.0, Fig. 2). For pH 6.0, the fluorescence was almost completely recovered with the return of pH to neutral, but only partially recovered for pH 5.0 to 2.0 (Figs. 3 and S4). As confirmed by CD (Fig. 4) and SEC-SAXS (Fig. 7), this occurred because there was no modification in the secondary and tertiary structure of EGFP at pH 6.0, hence, this effect was likely due to changes caused by a reversible protonation. However, there was structural modification, even at the secondary structure level, from pH 5.0 to 2.0 (as can be seen by CD in Fig. 4 for pH 5.0 and below, in IFP in Fig. 5 for pH 3.0 and 2.0, and for pH 5.5 and lower in well-plate SAXS and SEC-SAXS, Figs. 6, 7 and S5). This can explain why the fluorescence dequenching was only partial below pH 6.0.

This observation is consistent with what has previously been observed for wtGFP, which has two protonated states and reversible fluorescence quenching from pH 5.5 to 12.0 due to an equilibrium between protonated and deprotonated states [14]. The results indicate EGFP presents the same behavior from pH 6.0 to 13.0, with state changes due to protonation causing reversible fluorescence quenching.

The irreversible fluorescence loss of another GFP variant (superfolder GFP, sfGFP) was previously studied using Nuclear Magnetic Resonance (NMR) by Andrews et al. [62]. The study presented experimental evidence that sfGFP chromophore flexibility is associated with the mispacking of intermediate states, where sfGFP folding under certain conditions can lead to a loosely packed or incorrect barrel. This effect can decrease the rigid of the structure necessary for fluorescence, [62] supporting why a fluorescent protein can recover its overall structure but still present irreversible fluorescence loss.

With this study, it was possible to update the knowledge regarding the fluorescence activity and structure of EGFP at different pH considering its two states, confirming EGFP is more similar to wtGFP than originally reported.

3.5. EGFP as analytical neutral to acidic pH-biosensors

Envisaging a further development of pH-biosensors, the relationship between EGFP fluorescence and pH was determined, assessing the viability of using EGFP as analytical tool. For that purpose, EGFP FI in the pH range from 3 to 9 was further evaluated. Fig. 8 shows the fitting of the sigmoidal curve to a growth/sigmoidal dose response model. [63] From this sigmoidal curve, it was possible to determine the pKa of 5.69 for EGFP, identical to the pKa of 5.7 previously found by Bomati et al. [63] for the same GFP variant.

The fit of the sigmoidal curve for EGFP had a $R^2 > 0.99$, and small variations of pH produced discernable variations in the FI, particularly in the range of 5–8. Considering some relevant diseases like tumors and joint diseases can present a decrease in pH around the afflicted areas (with the average pH for tumors around 7.0, and for healthy tissues around 7.4) [35–37], there is a strong potential for application of EGFP in the development of biosensors for these conditions.

4. Conclusion

This study provides an update on previous knowledge regarding EGFP behavior at different pH and is in accordance with recent studies on the crystalline structure and fluorescence properties of EGFP. This further confirms the similarities between EGFP and wtGFP, with both having protonated and deprotonated states which cause reversible fluorescence quenching. This knowledge, allied with the strong dependence of EGFP fluorescence on pH also confirms that this protein presents the required properties for the development of novel biocompatible and environmentally friendly neutral-to-acidic pH-biosensors.

Abbreviations

λ_{em}	wavelength of emission
λ_{ex}	wavelength of excitation
EGFP	enhanced GFP
F1	EGFP fluorescence peak at λ_{ex} 488 nm and λ_{em} at 510 nm (highest intensity peak)
FI	fluorescence intensity
IFP	intrinsic fluorescence of proteins
PB	potassium phosphate buffer
Phe	phenylaniline
SAXS	small angle X-ray scattering
SEC-SAXS	size-exclusion chromatography SAXS
Trp	tryptophan
Tyr	tyrosine
UF	units of fluorescence
wtGFP	wild-type GFP

CRediT authorship contribution statement

JFBP proposed and designed the study; NVS and JFBP drafted paper; NVS and CFS conducted the experiments; NVS, TLG and JFBP planned the experiments and analyzed data; TLG and TMR coordinated the SAXS experiments and data analysis; FLP helped with discussion and analysis of results; TLG and JFBP were responsible for funding acquisition and supervision. All authors collaborated with the discussions of results, review and editing of the original manuscript.

Declaration of competing interest

There are no conflicts of interest in this work.

Acknowledgements

This work was developed within the scope of the project "Understanding the molecular interactions between ionic liquids and biopharmaceuticals: the key for a proper design of downstream processing", 2018/50009-8, co-funded by FAPESP (São Paulo Research

Foundation, Brazil) and Australian Technology Network of Universities (ATN) and projects FAPESP 2014/19793-3 and 2014/16424-7. N.V. Santos (2016/07529-5 and 18/06576-5) and C.F. Saponi (2018/01858-2 and 2018/20833-0) acknowledge scholarships financial support from FAPESP. N. V. Santos and J.F.B. Pereira also acknowledge the funding from CNPq, CAPES (001) and CAPES-PROEX. The authors acknowledge the support of the ANSTO in providing time in the SAXS/WAXS beamline for this work (Proposal M14460).

Appendix A. Supplementary data

Supplementary data to this article can be found online at https://doi.org/10.1016/j.ijbiomac.2020.08.224.

References

[1] L. Poppenborg, K. Friehs, E. Flaschel, The Green Fluorescent Protein is a versatile reporter for bioprocess monitoring, J. Biotechnol. 58 (1997) 79–88.
[2] R.Y. Tsien, The Green Fluorescent Protein, Annu. Rev. Biochem. 67 (1998) 509–544.
[3] S.J. Remington, Green Fluorescent Protein: a perspective, Protein Sci. 20 (2011) 1509–1519.
[4] K.A. Giuliano, P.L. Post, K.M. Hahn, D.L. Taylor, Fluorescent protein biosensors: measurement of molecular dynamics in living cells, Annu. Rev. Biophys. Biomol. Struct. 24 (1995) 405–434.
[5] K.A. Giuliano, D.L. Taylor, Fluorescent-protein biosensors: new tools for drug discovery, Trends Biotechnol. 16 (1998) 135–140.
[6] J.A. Arpino, P.J. Rizkallah, D.D. Jones, Crystal structure of enhanced Green Fluorescent Protein to 1.35 Å resolution reveals alternative conformations for Glu222, PLoS One 7 (2012), e47132.
[7] A. Royant, M. Noirclerc-Savoye, Stabilizing role of glutamic acid 222 in the structure of Enhanced Green Fluorescent Protein, J. Struct. Biol. 174 (2011) 385–390.
[8] T.N. Campbell, F.Y. Choy, The effect of pH on Green Fluorescent Protein: a brief review, Molecular Biology Today. 2 (2001) 1–4.
[9] J. Krasowska, M. Olasek, A. Bzowska, P.L. Clark, B. Wielgus-Kutrowska, The comparison of aggregation and folding of Enhanced Green Fluorescent Protein (EGFP) by spectroscopic studies, Journal of Spectroscopy. 24 (2010) 343–348.
[10] G.H. Patterson, S.M. Knobel, W.D. Sharif, S.R. Kain, D.W. Piston, Use of the green fluorescent protein and its mutants in quantitative fluorescence microscopy, Biophys. J. 73 (1997) 2782.
[11] M. Zimmer, Green Fluorescent Protein (GFP): applications, structure, and related photophysical behavior, Chem. Rev. 102 (2002) 759–782.
[12] S. Enoki, K. Saeki, K. Maki, K. Kuwajima, Acid denaturation and refolding of Green Fluorescent Protein, Biochemistry. 43 (2004) 14238–14248.
[13] F. Yang, L.G. Moss, G.N. Phillips, The molecular structure of Green Fluorescent Protein, Nat. Biotechnol. 14 (1996) 1246–1251.
[14] W.W. Ward, H.J. Prentice, A.F. Roth, C.W. Cody, S.C. Reeves, Spectral perturbations of the *Aequorea* green-fluorescent protein, Photochem. Photobiol. 35 (1982) 803–808.
[15] J. Farrell, A. Rose, Temperature effects on microorganisms, Annual Reviews in Microbiology 21 (1967) 101–120.
[16] R.J. Masterton, C.M. Smales, The impact of process temperature on mammalian cell lines and the implications for the production of recombinant proteins in CHO cells, Pharmaceutical Bioprocessing 2 (2014) 49–61.
[17] B.P. Cormack, R.H. Valdivia, S. Falkow, FACS-optimized mutants of the Green Fluorescent Protein (GFP), Gene 173 (1996) 33–38.
[18] H.M. Berman, T. Battistuz, T.N. Bhat, W.F. Bluhm, P.E. Bourne, K. Burkhardt, Z. Feng, G.L. Gilliland, L. Iype, S. Jain, The protein data bank, Acta Crystallogr. D Biol. Crystallogr. 58 (2002) 899–907.
[19] E.F. Pettersen, T.D. Goddard, C.C. Huang, G.S. Couch, D.M. Greenblatt, E.C. Meng, T.E. Ferrin, UCSF chimera—a visualization system for exploratory research and analysis, J. Comput. Chem. 25 (2004) 1605–1612.
[20] C. Lopes, N.V. dos dos Santos, J. Dupont, D.B. Pedrolli, S.R. Valentini, V. de C. Santos-Ebinuma, J.F.B. Pereira, Improving the cost effectiveness of enhanced green fluorescent protein production using recombinant *Escherichia coli* BL21 (DE3): decreasing the expression inducer concentration, Biotechnol. Appl. Biochem. 66 (2019) 527–536, https://doi.org/10.1002/bab.1749.
[21] R. Heim, A.B. Cubitt, R.Y. Tsien, Improved green fluorescence, Nature 373 (1995) 663–664.
[22] M.J. Mahon, pHluorin2: an enhanced, ratiometric, pH-sensitive Green Florescent Protein, Adv. Biosci. Biotechnol. 2 (2011) 132.
[23] G.T. Hanson, T.B. McAnaney, E.S. Park, M.E. Rendell, D.K. Yarbrough, S. Chu, L. Xi, S.G. Boxer, M.H. Montrose, S.J. Remington, Green Fluorescent Protein variants as ratiometric dual emission pH sensors. 1. Structural characterization and preliminary application, Biochemistry 41 (2002) 15477–15488.
[24] D.E. Johnson, H. Ai, P. Wong, J.D. Young, R.E. Campbell, J.R. Casey, Red fluorescent protein pH biosensor to detect concentrative nucleoside transport, J. Biol. Chem. 284 (2009) 20499–20511.
[25] S. Higson, Biosensors for Medical Applications, 1st ed. Woodhead Publishing, Cambridge, UK, 2012.
[26] M. Burnworth, S.J. Rowan, C. Weder, Fluorescent sensors for the detection of chemical warfare agents, Chem. Eur. J. 13 (2007) 7828–7836.
[27] K.P. Carter, A.M. Young, A.E. Palmer, Fluorescent sensors for measuring metal ions in living systems, Chem. Rev. 114 (2014) 4564–4601.
[28] D.W. Domaille, E.L. Que, C.J. Chang, Synthetic fluorescent sensors for studying the cell biology of metals, Nat. Chem. Biol. 4 (2008) 168.
[29] G.A. Lutty, The acute intravenous toxicity of biological stains, dyes, and other fluorescent substances, Toxicol. Appl. Pharmacol. 44 (1978) 225–249.
[30] R. Hardman, A toxicologic review of quantum dots: toxicity depends on physicochemical and environmental factors, Environ. Health Perspect. 114 (2006) 165–172.
[31] A. Shiohara, A. Hoshino, K. Hanaki, K. Suzuki, K. Yamamoto, On the cyto-toxicity caused by quantum dots, Microbiol. Immunol. 48 (2004) 669–675.
[32] D.M. Chudakov, M.V. Matz, S. Lukyanov, K.A. Lukyanov, Fluorescent proteins and their applications in imaging living cells and tissues, Physiol. Rev. 90 (2010) 1103–1163.
[33] H.-H. Gerdes, C. Kaether, Green fluorescent protein: applications in cell biology, FEBS Lett. 389 (1996) 44–47.
[34] R. Alford, H.M. Simpson, J. Duberman, G.C. Hill, M. Ogawa, C. Regino, H. Kobayashi, P.L. Choyke, Toxicity of organic fluorophores used in molecular imaging: literature review, Mol. Imaging 8 (2009) 7290–2009.
[35] I.F. Tannock, D. Rotin, Acid pH in tumors and its potential for therapeutic exploitation, Cancer Res. 49 (1989) 4373–4384.
[36] J.L. Wike-Hooley, J. Haveman, H.S. Reinhold, The relevance of tumour pH to the treatment of malignant disease, Radiother. Oncol. 2 (1984) 343–366.
[37] P.S. Treuhaft, D.J. McCarty, Synovial fluid pH, lactate, oxygen and carbon dioxide partial pressure in various joint diseases, Arthritis & Rheumatism: Official Journal of the American College of Rheumatology. 14 (1971) 475–484.
[38] S. Wack, A. Hajri, F. Heisel, M. Sowinska, C. Berger, M. Whelan, J. Marescaux, M. Aprahamian, Feasibility, sensitivity, and reliability of laser-induced fluorescence imaging of green fluorescent protein-expressing tumors in vivo, Mol. Ther. 7 (2003) 765–773.
[39] R. Ferreira, C. Pereira, S.F. Correia, M. Martins, O. Savchuk, J.A. Coutinho, P. André, J.B. Nieder, S.P. Ventura, Environmentally friendly luminescent solar concentrators based on optically efficient and stable green fluorescent protein, Green Chem. (2020)https://doi.org/10.1039/D0GC01742F.
[40] N.V. Dos Santos, M. Martins, V.C. Santos-Ebinuma, S.P. Ventura, J.A. Coutinho, S.R. Valentini, J.F. Pereira, Aqueous biphasic systems composed of cholinium chloride and polymers as effective platforms for the purification of recombinant green fluorescent protein, ACS Sustain. Chem. Eng. 6 (2018) 9383–9393.
[41] N.C. Shaner, P.A. Steinbach, R.Y. Tsien, A guide to choosing fluorescent proteins, Nat. Methods 2 (2005) 905–909.
[42] J.R. Lakowicz, Protein fluorescence, Principles of Fluorescence Spectroscopy, Springer 1983, pp. 341–381.
[43] N.J. Greenfield, Using circular dichroism spectra to estimate protein secondary structure, Nat. Protoc. 1 (2006) 2876.
[44] L. Whitmore, B.A. Wallace, Protein secondary structure analyses from circular dichroism spectroscopy: methods and reference databases, Biopolymers: Original Research on Biomolecules. 89 (2008) 392–400.
[45] L. Whitmore, B.A. Wallace, DICHROWEB, an online server for protein secondary structure analyses from circular dichroism spectroscopic data, Nucleic Acids Res. 32 (2004) W668–W673.
[46] J.G. Lees, A.J. Miles, F. Wien, B.A. Wallace, A reference database for circular dichroism spectroscopy covering fold and secondary structure space, Bioinformatics 22 (2006) 1955–1962.
[47] T.M. Ryan, J. Trewhella, J.M. Murphy, J.R. Keown, L. Casey, F.G. Pearce, D.C. Goldstone, K. Chen, Z. Luo, B. Kobe, An optimized SEC-SAXS system enabling high X-ray dose for rapid SAXS assessment with correlated UV measurements for biomolecular structure analysis, J. Appl. Crystallogr. 51 (2018) 97–111.
[48] J. Trewhella, A.P. Duff, D. Durand, F. Gabel, J.M. Guss, W.A. Hendrickson, G.L. Hura, D.A. Jacques, N.M. Kirby, A.H. Kwan, 2017 publication guidelines for structural modelling of small-angle scattering data from biomolecules in solution: an update, Acta Crystallographica Section D: Structural Biology 73 (2017) 710–728.
[49] ANSTO – Australian Synchrotron, SAXS specifications, http://archive.synchrotron.org.au/index.php?option=com_content&view=article&id=218&catid=36&Itemid=391 2020. (Accessed 31 January 2020).
[50] ANSTO – Australian Synchrotron, SAXS software, http://archive.synchrotron.org.au/aussyncbeamlines/saxswaxs/software-saxswaxs 2020. (Accessed 6 February 2020).
[51] D. Franke, M.V. Petoukhov, P.V. Konarev, A. Panjkovich, A. Tuukkanen, H.D.T. Mertens, A.G. Kikhney, N.R. Hajizadeh, J.M. Franklin, C.M. Jeffries, ATSAS 2.8: a comprehensive data analysis suite for small-angle scattering from macromolecular solutions, J. Appl. Crystallogr. 50 (2017) 1212–1225.
[52] A. Panjkovich, D.I. Svergun, Deciphering conformational transitions of proteins by small angle X-ray scattering and normal mode analysis, Phys. Chem. Chem. Phys. 18 (2016) 5707–5719.
[53] H.M. Berman, J. Westbrook, Z. Feng, G. Gilliland, T.N. Bhat, H. Weissig, I.N. Shindyalov, P.E. Bourne, The Protein Data Bank Nucleic Acids Research, vol. 28, 2000 235–242 , URL Www.Rcsb.OrgCitation.
[54] V. Postupalenko, A.-P. Sibler, D. Desplancq, Y. Nominé, D. Spehner, P. Schultz, E. Weiss, G. Zuber, Intracellular delivery of functionally active proteins using self-assembling pyridylthiourea-polyethylenimine, J. Control. Release 178 (2014) 86–94.
[55] P. Zhang, Y. Hu, R. Ma, L. Li, J. Lu, Enhanced Green Fluorescence Protein/layered double hydroxide composite ultrathin films: bio-hybrid assembly and potential application as a fluorescent biosensor, J. Mater. Chem. B 5 (2017) 160–166.
[56] M.R. Eftink, Intrinsic fluorescence of proteins, Topics in Fluorescence Spectroscopy, Springer 2002, pp. 1–15.

[57] S. Gurunathan, J.W. Han, E. Kim, D.-N. Kwon, J.-K. Park, J.-H. Kim, Enhanced Green Fluorescent Protein-mediated synthesis of biocompatible graphene, Journal of Nanobiotechnology 12 (2014) 41.
[58] E.Y. Chi, S. Krishnan, T.W. Randolph, J.F. Carpenter, Physical stability of proteins in aqueous solution: mechanism and driving forces in nonnative protein aggregation, Pharm. Res. 20 (2003) 1325–1336.
[59] C.N. Pace, F. Vajdos, L. Fee, G. Grimsley, T. Gray, How to measure and predict the molar absorption coefficient of a protein, Protein Sci. 4 (1995) 2411–2423.
[60] E.P. Melo, M.R. Aires-Barros, S.M.B. Costa, J.M.S. Cabral, Thermal unfolding of proteins at high pH range studied by UV absorbance, J. Biochem. Biophys. Methods 34 (1997) 45–59.
[61] D.P. Myatt, L. Hatter, S.E. Rogers, A.E. Terry, L.A. Clifton, Monomeric Green Fluorescent Protein as a protein standard for small angle scattering, Biomedical Spectroscopy and Imaging 6 (2017) 123–134.
[62] B.T. Andrews, M. Roy, P.A. Jennings, Chromophore packing leads to hysteresis in GFP, J. Mol. Biol. 392 (2009) 218–227.
[63] E.K. Bomati, J.E. Haley, J.P. Noel, D.D. Deheyn, Spectral and structural comparison between bright and dim green fluorescent proteins in Amphioxus, Sci. Rep. 4 (2014) 5469.